Geophysical Research Letters

RESEARCH LETTER
10.1029/2018GL077869

Vertical Structure of Diurnal Englacial Hydrology Cycle at Helheim Glacier, East Greenland

Irena Vaňková[1,2], Denis Voytenko[1,2], Keith W. Nicholls[3], Surui Xie[4], Byron R. Parizek[5,6], and David M. Holland[1,2]

[1]Courant Institute of Mathematical Sciences, New York University, New York, NY, USA, [2]Center for Global Sea Level Change, New York University, Abu Dhabi, UAE, [3]British Antarctic Survey, Natural Environment Research Council, Cambridge, UK, [4]School of Geosciences, University of South Florida, Tampa, FL, USA, [5]Mathematics and Geoscience, Pennsylvania State University, DuBois, PA, USA, [6]Department of Geosciences, Pennsylvania State University, University Park, PA, USA

Key Points:
- Observations of the interior of an outlet glacier recorded with an autonomous phase-sensitive radio-echo sounder (ApRES) reveal a diurnal meltwater cycle with a complex vertical structure
- The amplitude of the diurnal meltwater cycle inside the glacier and the hydraulic surface-to-base connectivity increase toward the calving front
- ApRES is demonstrated to be a suitable instrument for the study of englacial hydrology

Supporting Information:
- Supporting Information S1
- Data Set S1
- Data Set S2

Correspondence to:
I. Vaňková,
vankova@cims.nyu.edu

Citation:
Vaňková, I., Voytenko, D., Nicholls, K. W., Xie, S., Parizek, B. R., & Holland, D. M. (2018). Vertical structure of diurnal englacial hydrology cycle at Helheim Glacier, East Greenland. *Geophysical Research Letters*, *45*, 8352–8362. https://doi.org/10.1029/2018GL077869

Received 9 MAR 2018
Accepted 12 JUL 2018
Accepted article online 24 JUL 2018
Published online 30 AUG 2018

©2018. American Geophysical Union. All Rights Reserved.

Abstract The interior dynamics of Helheim Glacier were monitored using an autonomous phase-sensitive radio-echo sounder (ApRES) during two consecutive summers. The return signals from all observational sites exhibited strong non-tidal, depth-dependent diurnal variations. We show that these variations in the glacier interior can be explained by an englacial diurnal meltwater cycle: a data interpretation that assumes constant ice-column composition through time leads to dynamical inconsistencies with concurrent observations from GPS and terrestrial radar. The observed diurnal meltwater cycle is spatially variable, both between different sites and in the vertical, consistent with the existence of a dense and complex englacial hydrologic network. Future applications of this observational technique could reveal long-term meltwater behavior inside glaciers and ice sheets, leading to an improved understanding of the spatiotemporal evolution of the basal boundary conditions needed to simulate them realistically.

Plain Language Summary Realistic glacier models require accurate description of the material properties of glacial ice and of its behavior at the boundaries. Meltwater transport through the glacier plays an important role in controlling these material properties and boundary conditions. However, the glacial interior is underobserved in both space and time and little is known about how this meltwater transport occurs. We used a new type of radar to monitor the interior of a Greenland outlet glacier to gain insight of its meltwater behavior. We found that the amount of meltwater present inside the glacier column changes through the day, and this daily meltwater cycle can occur at all depths of the glacier. Our observations indicate that the hydrologic network inside a glacier is dense and complex.

1. Introduction

The Greenland Ice Sheet (GrIS) is an important component of the climate system, yet attempts to model it suffer from our limited knowledge of the boundary conditions at its base and at its seaward margin (Vaughan & Arthern, 2007). The basal boundary conditions control glacier flow and are sensitive to changes in the volume (Schoof, 2010) and location (Parizek & Alley, 2004) of surface meltwater transport to the bed, which is thought to occur primarily via crevasses and moulins formed by hydrofracture at regions where meltwater supply is abundant and surface stresses are high (Alley et al., 2005; Boon & Sharp, 2003). Hourly to seasonal changes in glacier surface velocities have been related to changes in the amount of meltwater at the glacier base (Bartholomew et al., 2010, 2012; Das et al., 2008; Zwally et al., 2002). Further, at alpine glaciers diurnal subglacial meltwater changes have been inferred from radar observations of diurnal changes in the nature of the basal reflector and attributed to englacially routed surface melt (Kulessa et al., 2008). However, processes in the glacier interior, which control the surface-to-bed meltwater transport across all of these timescales remain underobserved. Knowledge of the glacier interior of the GrIS comes from borehole measurements at slower moving regions of the ice sheet (Lüthi et al., 2002; Ryser et al., 2014) and from ice-penetrating radar observations (Bell et al., 2014; Catania et al., 2008), which have good spatial but limited temporal coverage. To extend our knowledge-base of this environment, we collected minute-by-minute observations with an autonomous phase-sensitive radio-echo sounder (ApRES) at four locations near the terminus of Helheim Glacier, a large and

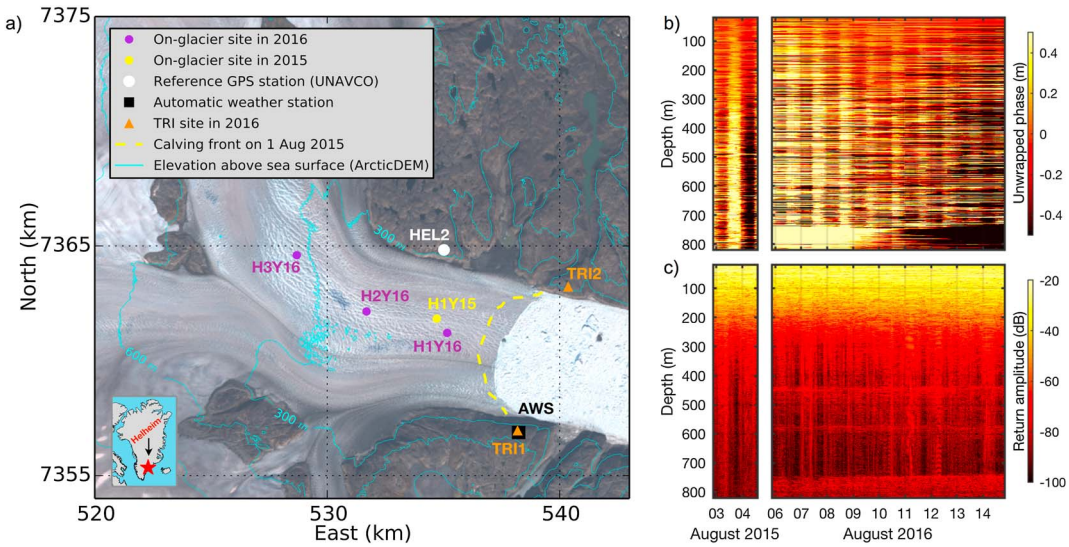

Figure 1. (a) Helheim Glacier with deployment sites (background image from Landsat-8 on 19 August 2016). (b) Unwrapped phase and (c) return amplitude from unfiltered ApRES data at H1Y15 (left) and H1Y16 (right). TRI = terrestrial radar interferometer.

fast-flowing outlet glacier in East Greenland. ApRES and its predecessor pRES have been successfully used to obtain high-precision measurements of basal melt rates and vertical strain rates in Antarctica (Corr et al., 2002; Nicholls et al., 2015). Here we explore the utility of this observational technique in a more dynamic, Greenland outlet glacier environment.

2. Methods

In August 2015, we conducted a pilot study in which we deployed one ApRES unit for 2 days ~2 km from Helheim's calving front, at site H1Y15 (Figure 1). In August 2016, we deployed three ApRES units, which collected data for 9–14 days. The instruments were placed ~4 km apart along a flow line at sites H1Y16, H2Y16, and H3Y16; the near-glacier front site H1Y16 was within ~600 m of H1Y15. GPS units were collocated at each of the four installations to provide a spatial reference for the ApRES Lagrangian measurement. All instruments were placed on the glacier in boxes fitted with crampons. Additionally, in 2016 a terrestrial radar interferometer (TRI) was installed on each side of the fjord to monitor the final ~5 km of the glacier surface. Thus, H1Y16 was well within the view of the TRIs, but H2Y16 and H3Y16 were farther upstream and out of their view. An automatic weather station near the glacier front recorded air temperature and incoming shortwave radiation during both years; a sea-floor mooring ~30 km down the fjord monitored sea surface displacements with a pressure sensor.

ApRES is a phase-sensitive radar that operates at a center frequency of 300 MHz (1-m wavelength in air), and its angle of view in ice is ~30° either side of nadir (technical specifications are described in Brennan et al. (2014)). ApRES detects internal reflectors inside the conical section of a glacier (i.e., glacier cone; Figure 4) viewed over a two-way-travel time based on the change in electromagnetic properties of the material. The relative motion of individual internal reflectors can be calculated by differencing the phase between subsequent measurements (Nicholls et al., 2015). Assuming constant composition of the glacier cone, the unwrapped phase of the return signal is used to convert changes in radio-wave travel time to displacement time series of depth-cumulative motion of internal reflectors above. Each ApRES sampled at 1-min intervals and the data were processed following Brennan et al. (2014) and Nicholls et al. (2015). Typical uncertainties estimated from signal-to-noise ratio were ~0.3 mm in the top 200–300 m and then increased with depth until at most 30 mm for H1Y16 and H1Y15 and at most 10 mm for H2Y16 and H3Y15.

The TRIs were used to generate line-of-sight velocity maps from line-of-sight displacements constructed by comparing the phase of subsequent measurements (Caduff et al., 2015; Voytenko et al., 2015). Between 6 and 11 August 2016 the two TRIs operated simultaneously, across the fjord from each other, in a near-optimal imaging configuration for constructing a 2-D glacier surface velocity field following Voytenko et al. (2017). Uncertainties, estimated based on a reference nonmoving target, were 0.6 and 1.0 m/day for the east-west

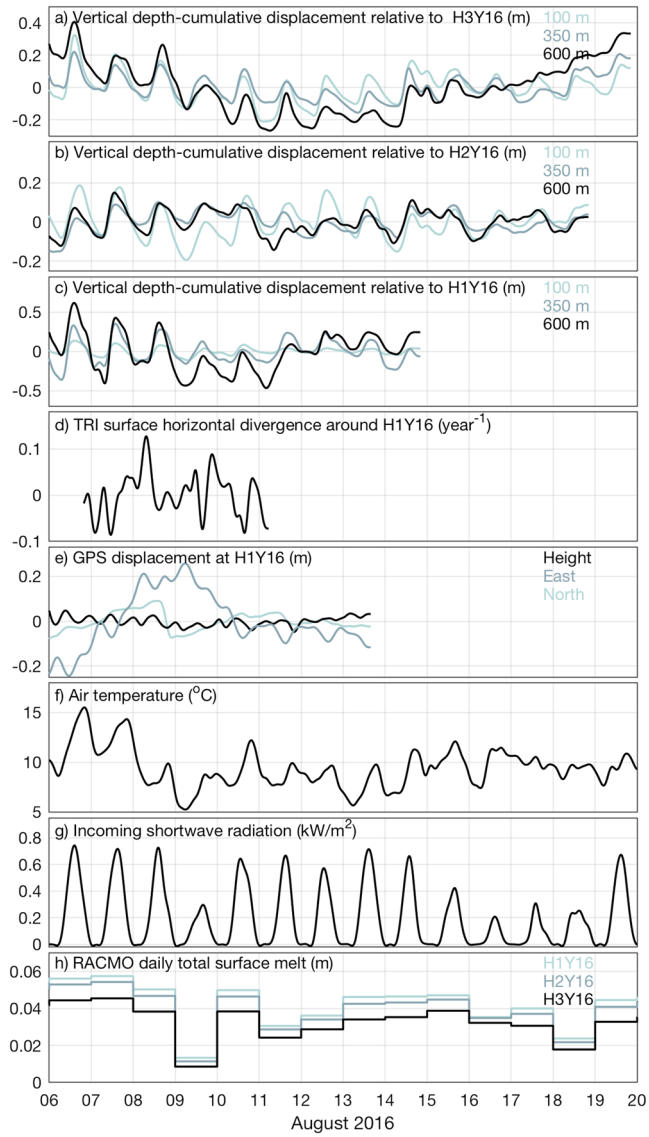

Figure 2. Time series from August 2016. Linear trend was removed from signal in panels (a)–(e). (a–c) Examples of ApRES depth-cumulative displacements at different depths. (d) TRI horizontal divergence at H1Y16. (e) GPS displacement at H1Y16. (f, g) Air temperature and incoming shortwave radiation at nearby station. (h) RACMO2.3p2 daily total surface melt.

and north-south velocity components, respectively. The velocity maps, available at 2-min intervals, were first averaged over 30-min segments to reduce spatial gaps arising as a result of line-of-sight obstacles on the irregular glacier surface (i.e., crevasses). Permanent spatial gaps in the data were filled using inward interpolation. The velocity maps were spatially smoothed via a combination of median and Gaussian filters and then used to calculate surface horizontal divergence.

The on-glacier GPS data were analyzed using the TRACK version 1.30 kinematic processing software (Chen, 1998), yielding position time series relative to a rock-based site HEL2 at 30-s intervals. To minimize potential jumps at boundaries of each day, for each session, we processed 48 hr of data centering at the middle of each day then removed position estimates the day before and after. Typical uncertainties in the horizontal coordinates were 3–6 mm, and in the vertical component 2–3 times larger.

We do not have concurrent measurements of surface melt and therefore rely on the daily RACMO2.3p2 output (Noël et al., 2018). The modeled mean surface melt near the terminus agrees well with values previously found by Andersen et al. (2010) for the summers 2007 and 2008. Assuming melt rate varies sinusoidally through

the day with the mean melt rate of ~0.044 m/day (RACMO2.3p2 for H1Y16), the diurnal peak-to-peak vertical displacement is ~0.01 m (Figure S6 in the supporting information).

To focus on diurnal variations in the ApRES, GPS, and TRI signals, a linear trend was removed from each time series, which were then low-pass filtered with a 6-hr fourth-order Butterworth filter (Figure 2). To extract the amplitude of the ApRES diurnal variations in the depth-cumulative displacement time series, these time series were first vertically averaged into 10-m depth bins (if strong off-nadir reflectors are present, a depth bin may consist of ice at different depths) and then low-pass filtered. A composite diurnal variation for each depth bin was then formed by splitting the time series into 1-day segments, subtracting the line connecting the starting and ending point from each segment (end points were chosen to correspond to diurnal minimum ice thickness occurring at 5 a.m. local time), and pointwise averaging over the segments to get the amplitude and standard deviation of the mean diurnal variation (Figures S3–S5). The same time interval (6–15 August) was used for all August 2016 stations, but only one 1-day segment was available for the 2015 deployment.

3. Results

A key feature of the ApRES return signal are diurnal variations, which are clearly visible even in the unfiltered data (Figures 1b, 1c, S7, and S8). Example time series of low-pass-filtered depth-cumulative displacements from the three August 2016 instruments are shown in Figures 2a–2c. The diurnal variations are in-phase with depth as well as between the three different sites. They are stronger at the glacier front and weaker at the two upstream sites, and their amplitude varies with depth. At the frontal sites, the diurnal amplitude of the depth-cumulative displacement could imply diurnal vertical strain rates of up to 1 year^{-1}, which would be an order of magnitude larger than the background vertical strain rate suggested by the ApRES data. Possible causes of these diurnal variations are investigated in section 4.

The amplitude of the diurnal variations as a function of depth is shown in Figure 3a. There is significant spatial variability in the vertical structure of these variations. At both H1Y15 and H1Y16 the diurnal amplitude increases with depth nearly linearly except for three large dips at H1Y16. At H2Y16 it increases linearly over the first 150 m but then sharply drops and remains approximately constant below 200 m. At H3Y16 the diurnal amplitude increases linearly to a depth of 200 m, then gradually decreases until 350 m, with little variation below this depth. Sharp drops in the diurnal amplitude observed at the three 2016 sites coincide with locations of enhanced amplitude (bright spots) of the return signal (Figure 3b). Since at each site the diurnal variations in depth-cumulative displacements are in-phase, a decrease in the diurnal amplitude with depth implies an out-of-phase behavior. The vertical structure of the diurnal variations is interpreted in section 5 once the diurnal forcing has been identified in section 4.

4. Causes of ApRES Diurnal Cycle

We consider the following explanations for the diurnal variations in the ApRES signal: instrument temperature sensitivity, ocean tidal forcing, ice dynamics, and changes in glacier meltwater content. Next, we show by the process of elimination that the only explanation consistent with the ApRES, GPS, and TRI instruments is that the observed diurnal variations are caused by changes in meltwater content inside the glacier.

4.1. Instrument Temperature Sensitivity

To test the temperature sensitivity of an ApRES, we reduced its temperature from 20° to −25° and the apparent change in length of 200 m of coaxial cable was monitored. This experiment showed that distance to a target appears ~0.3 mm greater if the ApRES is warmed by 1°. The amplitude of the observed diurnal variations is 1–2 orders of magnitude larger than any possible apparent ice extension due to diurnal temperature change. Further, the instrument's temperature sensitivity is largely depth independent; therefore, changes in the instrument temperature would result in a near-constant offset at the surface (same as surface melt) and cannot cause the depth-dependent diurnal variations that are observed at all sites.

4.2. Ocean Tidal Forcing

The ocean tidal forcing near Helheim's front is predominantly semidiurnal (Davis et al., 2014) with the M2 constituent being ~5.5 times stronger than the sum of the diurnal constituents (Figures S1 and S9). Both GPS (horizontal and vertical displacement) and TRI (surface horizontal divergence) show primarily semidiurnal motion, although their diurnal variations are enhanced compared with the amplitude of the ocean's diurnal

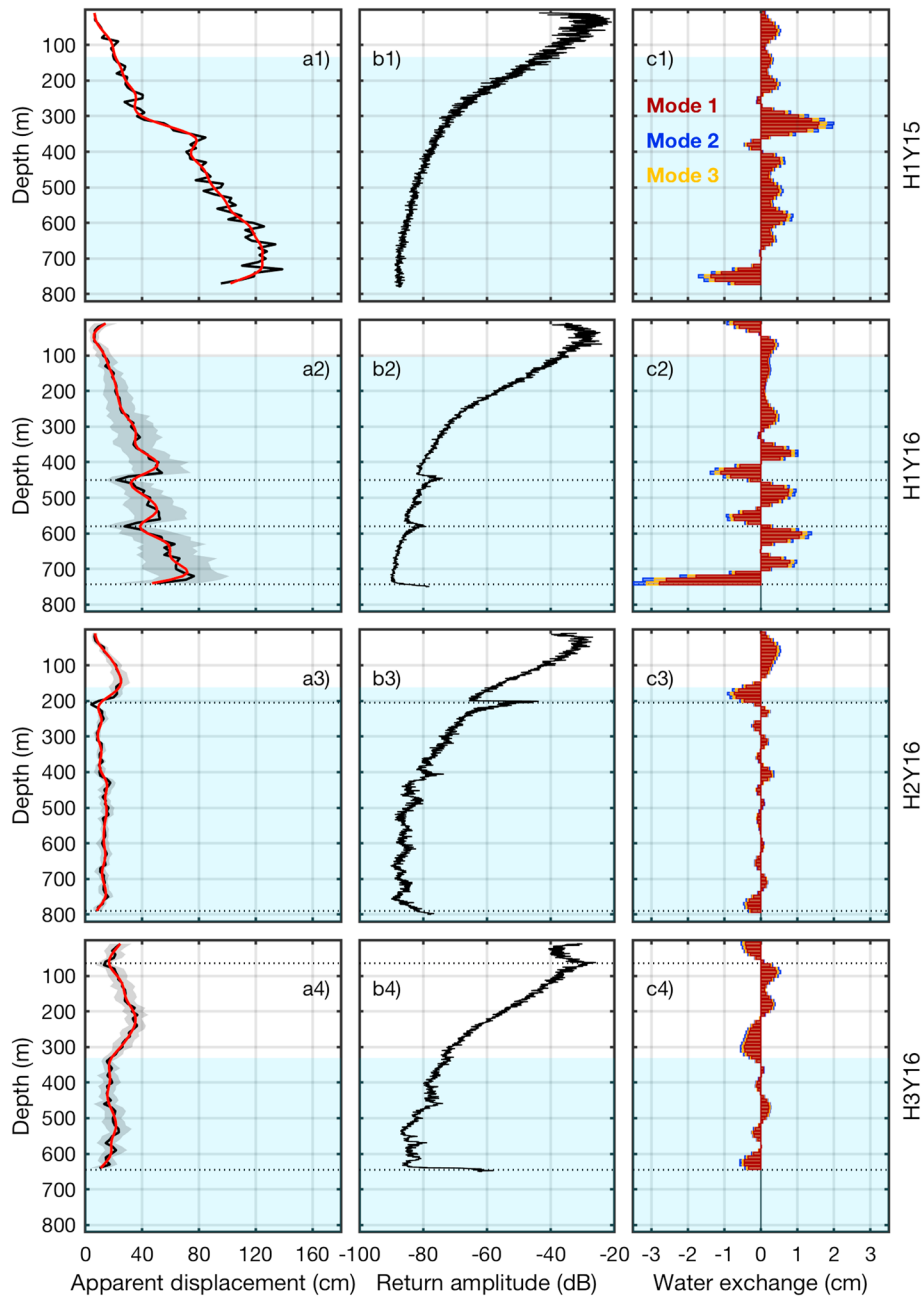

Figure 3. Vertical structure of the ApRES-derived diurnal variations. (a) Diurnal depth-cumulative peak-to-peak displacement of each 10-m depth bin; shaded region (shown for records longer than 1 day) lies within one standard deviation from the mean (black line). (b) Time average of the return signal amplitude; strong bright spots are highlighted with dotted line in all panels. (c) Mean diurnal meltwater exchange in each 10-m depth bin (based on low-pass-filtered orange line in column (a). Depth below sea surface is shaded in blue.

constituents. The ApRES signal is dominated by diurnal variations. Therefore, any potential tidally forced signal in the ApRES data is overshadowed by a much stronger, diurnal forcing of different origin.

4.3. Ice Dynamics

At H1Y16, there is a ~5 day overlap of ApRES, GPS, and the two TRIs. Since each instrument measures a different aspect of glacier motion, their combination allows us to investigate whether the diurnal variations in the ApRES signal could result from ice dynamics. If that were the case, the amplitudes of diurnal surface horizontal divergence (TRI), diurnal vertical strain rate (ApRES), and diurnal vertical displacement (GPS) would need to be consistent.

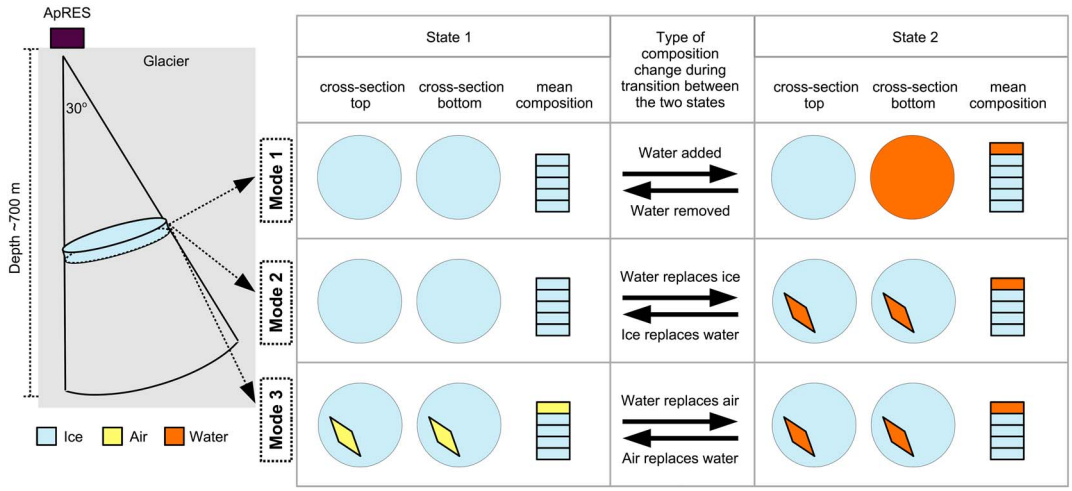

Figure 4. Schematic diagram showing independent modes of composition change due to meltwater cycle inside a cross section of a glacier cone viewed by the ApRES. Each mode goes between two states: State 1 containing the minimum amount of meltwater and State 2 containing the maximum. Mode 1—meltwater is added/removed as a horizontal layer, increasing/decreasing the cross-section thickness. Mode 2—meltwater replaces ice/ice replaces meltwater while cross-section thickness remains constant. Mode 3—meltwater replaces air/air replaces meltwater while cross-section thickness remains constant.

First, we compare the ApRES and TRI observations at H1Y16. A diurnal vertical ice extension implies a diurnal vertical strain rate w'_z superimposed on the background vertical strain rate w_z. To relate w'_z to the diurnal horizontal divergence at the glacier surface $u'_x+v'_y$, we need to make the following assumptions: (a) the glacier is incompressible and (b) w'_z is constant with depth. Incompressibility is a good assumption as long as air and meltwater fractions in the glacier are small; whether that is the case at Helheim is a priori unknown. To a first approximation the diurnal amplitude of the depth-cumulative vertical displacements increases linearly with depth (Figure 3a2), which would imply a constant w'_z, should the diurnal variations be due to ice dynamics. With these assumptions $u'_x + v'_y$ compensates w'_z, following

$$u'_x + v'_y = -w'_z, \tag{1}$$

where $\vec{u}' = (u', v', w')$ is the diurnal perturbation of the background 3-D ice velocity field $\vec{u} = (u, v, w)$. Average w'_z over the time T during which the glacier goes from maximum vertical compression to maximum vertical extension is given by

$$\overline{w'_z} = \frac{\left(\frac{\Delta H'}{H}\right)}{T}, \tag{2}$$

where $\Delta H'$ is the vertically integrated ice extension at its peak and H is the glacier thickness at maximum compression. At H1Y16, the representative values are $H \sim 730$ m, $T \sim 0.5$ day, and $\Delta H' \sim 0.75$ m. These values give $\left|\overline{w'_z}\right| \sim 0.75$ year^{-1} and $\left|\overline{u'_x + v'_y}\right| \sim 0.75$ year^{-1} using (2) and (1), respectively. To compare with the TRI, we consider $\left|u'_x + v'_y\right|$ over a 200-m by 200-m box, which encloses the Lagrangian path traveled by H1Y16. Over this region $\left|u'_x + v'_y\right|$ reaches at most 0.1 year^{-1} (Figure 2d), implying an upper bound on the diurnal ice extension of $\Delta H' \leq 0.1$ m using (1) and (2). Thus, this upper bound is ~7.5 times smaller than the average ApRES-observed value of $\Delta H'$.

Next, we turn to the GPS data and investigate whether the ApRES-observed $\Delta H'$ at H1Y16 is reflected in the vertical displacement of the glacier surface. The GPS diurnal peak-to-peak vertical displacement is at most ~0.02 m (Figures 2e and S1), and maximum possible cancelation due to diurnal tidal constituents in the ocean forcing would be an order of magnitude smaller. Cancelations due to diurnal glacier surface melt can be up to ~0.01 m (see section 2). With that, the maximum diurnal vertical displacement amounts to ~0.03 m. Therefore, if H1Y16 were grounded, the maximum observable $\Delta H'$ would be only ~0.03 m, which is ~25 times smaller than observed. Otherwise, if H1Y16 were ungrounded and in hydrostatic balance, the vertical displacement of ~0.03 m would allow a maximum $\Delta H'$ of ~0.3 m, based on the density contrast between ice and sea water.

This value is ∼2.5 times smaller than observed. We note that with at least partial grounding of H1Y16 the GPS diurnal vertical displacement can satisfy the TRI-derived upper bound on $\Delta H'$ of 0.1 m. Present data are insufficient to assess whether the site H1Y16 is floating or grounded as vertical tidal signal does not necessarily imply flotation (de Juan et al., 2010). However, sites H2Y16 and H3Y16, which are farther upstream, are very likely grounded. These two sites behave similarly, showing the ApRES-derived $\Delta H' \sim 0.1$ m and diurnal peak-to-peak vertical displacement ∼0.02 m (accounting for surface melt). Therefore, at the upstream sites the vertical GPS displacement would need to be ∼5 times larger to explain the $\Delta H'$ observed by the ApRES.

We used the diurnal amplitudes of TRI-derived surface divergence and GPS-observed surface vertical displacement to derive upper bounds on the diurnal vertical ice extension. These upper bounds give values that are an order of magnitude smaller than the typical ApRES-observed vertical ice extension. Depth independency of the vertical strain rate is implied by the observed nearly linear increase of the diurnal variations with depth and cannot be relaxed. Allowing for crevasses increases the horizontal divergence required to produce the observed vertical extension; thus, relaxing the assumption about incompressibility cannot explain the discrepancy shown by the above calculations. We conclude that ice dynamics cannot explain the ApRES-observed diurnal variations.

4.4. Changes in Meltwater Content

We now investigate the effect that changes in the glacier meltwater content could have on the phase of the ApRES return signal and calculate the amount of water needed to produce the observed diurnal variations. The speed (v) of an electromagnetic wave through a medium is given by $v = \frac{c}{n}$, where c is the speed of light in a vacuum and n is the refractive index of the medium. Since n and therefore v are material dependent, temporal change in the glacier cone composition results in an apparent motion of the internal ice reflectors. At the 300-MHz center frequency at which ApRES operates, the refractive indices of water (n_w), glacial ice (n_g), and air (n_a) are 8.85, 1.78, and 1, respectively. When the ApRES data are processed and radio-wave travel time is converted to distance, n is assumed constant and equal to n_g. Since $n_w > n_g$ and $n_w > n_a$, it is always the case that an increase in meltwater fraction causes apparent vertical glacier extension. To quantify the amount of meltwater needed to produce the observed amplitude of the diurnal variations, we consider different ways by which meltwater can change the composition of the glacier cone viewed by ApRES. These can be conceptually decomposed into three independent modes (schematically shown in Figure 4). First, we analyze each mode individually to assess whether meltwater can explain the ApRES-observed diurnal cycle. Once this has been established, we discuss in section 5 how these modes relate to physical mechanisms. The apparent vertical depth-cumulative displacement $\Delta H'$ (measured by the ApRES) is related to the equivalent thickness of meltwater $\Delta H'_w$ by comparing radio-wave travel time (RWTT) through the different states of composition each mode undergoes.

- Mode 1: Meltwater is added/removed in the vertical. The glacier thickness changes by $\Delta H'_w$, and its surface is displaced vertically, but there is no diurnal horizontal divergence. Before adding meltwater, the RWTT through the glacier is

$$t_{\text{back}} = H \cdot \frac{n_g}{c}. \tag{3}$$

After adding meltwater of $\Delta H'_w$ thickness, the new RWTT becomes

$$t'_w = t_{\text{back}} + \Delta H'_w \cdot \frac{n_w}{c}. \tag{4}$$

If added meltwater is misinterpreted as ice by assuming constant glacier cone composition, the recorded RWTT can be used to calculate $\Delta H'$ from

$$t' = t_{\text{back}} + \Delta H' \cdot \frac{n_g}{c}. \tag{5}$$

Finally, equating (5) and (4) relates $\Delta H'$ and $\Delta H'_w$:

$$\Delta H'_w = \frac{\Delta H' \cdot n_g}{n_w}. \tag{6}$$

- Mode 2: Meltwater replaces/is replaced by ice. The glacier thickness remains constant, and the displaced ice moves horizontally in and out of the ApRES view implying horizontal divergence. Before meltwater is introduced, the RWTT through the glacier is given by (3). When $\Delta H'_w$ thickness of ice is replaced by meltwater the new RWTT becomes

$$t'_w = \left(H - \Delta H'_w\right) \cdot \frac{n_g}{c} + \Delta H'_w \cdot \frac{n_w}{c}. \tag{7}$$

The relation between $\Delta H'_w$ and $\Delta H'$ is found by equating (5) and (7):

$$\Delta H'_w = \frac{\Delta H' \cdot n_g}{n_w - n_g}. \tag{8}$$

- Mode 3: Meltwater replaces/is replaced by air. The glacier thickness remains constant, and there is no horizontal divergence. Before meltwater is introduced, RWTT is

$$t_{\text{back}} = \left(H - \Delta H'_w\right) \cdot \frac{n_g}{c} + \Delta H'_w \cdot \frac{n_a}{c}. \tag{9}$$

When $\Delta H'_w$ thickness of air is replaced by meltwater, it leads to a new RWTT

$$t'_w = \left(H - \Delta H'_w\right) \cdot \frac{n_g}{c} + \Delta H'_w \cdot \frac{n_w}{c}. \tag{10}$$

Again, equating (5) and (10) relates $\Delta H'_w$ and $\Delta H'$:

$$\Delta H'_w = \frac{\Delta H' \cdot n_g}{n_w - n_a}. \tag{11}$$

The ApRES-observed $\Delta H' \sim 0.75$ m at H1Y16 requires $\Delta H'_w$ ~0.15, 0.19, and 0.17 m for Modes 1, 2, and 3, respectively. Additionally, Mode 1 requires a diurnal vertical displacement of ~0.15 m if grounded or by ~0.015 m if afloat. With the assumption of depth independence we can estimate the $\left|\overline{u'_x + v'_y}\right|$ required by Mode 2 by combining (1) and (2) and setting $\Delta H' = \Delta H'_w$. This gives $\left|\overline{u'_x + v'_y}\right| \sim 0.19\,\text{year}^{-1}$, which is twice the maximum value of the observed diurnal surface divergence. However, having established that the nearly linear increase in the diurnal variations with depth is not indicative of constant vertical strain rate (see section 4.3), we cannot argue that depth independence of horizontal divergence is a good assumption; in fact, at some glaciers there exists direct evidence that it is not (Pfeffer et al., 2000). As a result we cannot use the bounds from section 4.3 to establish which of the modes dominates.

The amount of meltwater needed to explain the ApRES-observed $\Delta H'$ is comparable for all three modes. At H1Y16 the required diurnal thickness change in meltwater for the full glacier thickness amounts to 0.15–0.19 m/day. Although this value is 3–4 times larger than the mean surface melt estimate of 0.044 m/day, it is reasonable to expect higher englacial meltwater cycle near the terminus where meltwater is collected from the much larger upstream catchment area. We conclude that diurnal meltwater englacial cycle can fully explain the observed diurnal variations.

5. Interpretation of Meltwater Cycle

To interpret the vertical structure of the diurnal variations, we discuss known physical mechanisms by which meltwater can appear/disappear from the glacier cone. These include the following:

- P1: Water fills/drains from preexisting air-filled cracks (Mode 3). Surface crevasses are a fundamental entry point for surface meltwater inside the glacier (Colgan et al., 2016). We expect this process to be important at Helheim, since its surface is heavily fractured. It should dominate above the sea surface, but below that its action will be limited if the englacial network is well connected with the ocean preventing water drainage.
- P2: Preexisting water-filled near-vertical cracks (moulins, basal crevasses, or network of fractures) widen/shrink, or new ones open/close (Mode 2). Full-depth and partial-depth penetrating moulins have been observed at the ablation zone of GrIS by Catania et al. (2008), who found strong correlation between moulin density and elevated surface tensile stresses associated with crevassing. Based on this result, we

would expect high moulin density in our study region. Existence of basal crevasses near Helheim front was inferred from glacier surface observations by James et al. (2014). These basal crevasses can have high water-storage capacity and may extend deep inside the glacier; for example, Harper et al. (2010) found that on a ∼200-m-thick Alaskan glacier water-filled basal crevasses penetrated tens of meters above the bed and contained ∼10 cm equivalent of water. A hydrological system dominated by fractures at all depths, with a slow circulation of water, was observed at Storglaciären (Sweden) by Fountain et al. (2005).

- P3: Preexisting water-filled horizontal layers (e.g., meltwater at the base or englacial lakes) widen/shrink, or new ones open/close (Mode 1). Support for this mechanism to act at the base of Helheim comes from Andersen et al. (2010) who observed a dependency of surface glacier velocities on runoff variations and attributed this to meltwater-induced diurnal changes at the base.
- P4: Preexisting water-filled horizontal channels widen/shrink, or new channels open/close (Modes 1 and 2). Englacial channels have been observed at many glaciers directly (Benn et al., 2009; Gulley & Benn, 2007) or using surface-based methods (Bælum & Benn, 2011; Moorman & Michel, 2000; Stuart et al., 2003). A channelized englacial network has not been directly observed at Helheim; however, its existence could explain observed surface lake drainage patterns (Everett et al., 2016) and flow speeds inside a firn aquifer located ∼60 km West from H3Y16 (Miller et al., 2018).
- P5: Water inside a glacier freezes/ice inside a glacier melts (Mode 1 and/or 2). Catania et al. (2008) directly observed refrozen meltwater inside moulins. Bell et al. (2014) used airborne radar observations to infer the presence of large units of refrozen basal water all over Greenland. Diurnally, melting and refreezing could act at Helheim as a result of variations in meltwater flow through englacial channels, although direct observations to confirm this are lacking. Further, diurnal melting and refreezing is expected to take place at the base of surface crevasses (Fountain & Walder, 1998).

Different mechanisms of meltwater exchange are likely to prevail at different parts of the glacier. Therefore, we consider all four ApRES data sets to gain further insight into the vertical structure of the diurnal water cycle and its spacial characteristics. The diurnal variations in apparent depth-cumulative displacements are in-phase at all depths for each ApRES. This implies that the meltwater cycle at all depths is either exactly in-phase (depth-cumulative displacement increases) or exactly out-of-phase (depth-cumulative displacement decreases). As a result, the vertical gradient in the amplitude of the diurnal variations may be used to infer the strength of the diurnal meltwater cycle $\Delta H'_w\big|_{j+1/2}$ at a depth bin located between depth levels j and $j+1$. The different modes of diurnal meltwater exchange apply to each glacier parcel in the same way as they apply to the whole glacier cone. Thus, (6), (8), and (11) can be used to relate $\Delta H'_w\big|_{j+1/2}$ to $\Delta H'\big|_{j+1/2} = H'\big|_{j+1} - H'\big|_j$. The vertical profile of $\Delta H'_w$ is plotted for each mode in Figure 3c. A change in sign with depth indicates phase reversal with respect to the depth bin directly above. There are various explanations for the occurrence of phase reversal with depth:

- C1: There is a vertical hydraulic connection between the two consecutive depth bins, and an alternating pressure gradient drives water out of small cracks into larger channels and back again. However, this requires the glacier to be porous at great depths, for which there is no direct observational evidence.
- C2: There is no vertical hydraulic connection between the two consecutive depth bins (at the given site), and each depth bin is connected to a different source of meltwater—directly above or further upstream, at the surface or at the base. For example, if both surface and basal crevasses were present, their respective rate of diurnal filling/draining could be out-of-phase. Also, the phase of diurnal cycle inside an englacial/supraglacial conduit can be delayed compared with the phase of the cycle in a moulin nearby. Further, faster water flow through englacial channels could increase refreezing due to enhanced turbulent transfer of heat, which would result in a phase reversal of the meltwater cycle at the channel depth.
- C3: The meltwater cycle is in-phase at all depths, but the glacier composition is heterogenous and the return ApRES signal is dominated by off-nadir reflectors. For example, a water-filled horizontal channel is a strong reflector. Therefore, the depth-cumulative displacement time series corresponding to a channel depth will be controlled by meltwater changes along the line between the channel and the ApRES. These can substantially differ from the integrated view of the water content above or below the channel. Therefore, if the glacier were heterogenous, and the signal dominated by off-nadir reflectors, the meltwater change reported at each depth is specific to a particular section of the glacier cone, which can result in jumps in the apparent

strength of the depth-cumulative meltwater cycle. In this case Figure 3c would be indicative of the degree of heterogeneity of the glacier cone.

We now interpret the vertical profile at each site, relating it to the physical mechanisms of meltwater exchange (P1–P5) and possibilities of phase reversal with depth (C1–C3) listed above. Sometimes, various interpretations are equally likely, in which case we state them all.

The upstream sites H2Y16 and H3Y16 show a stronger diurnal meltwater cycle in the upper part of the glacier cone, and the cycle becomes weak below the sea surface. This indicates that air-meltwater exchange dominates at these sites (P1) and that much of the meltwater seen in the upper part of the glacier does not immediately reach the bed. Instead, it enters an englacial network which transports it further downstream. At both H2Y16 and H3Y16, there is a bright spot in the return signal coincidental with the change of phase of the diurnal meltwater exchange between consecutive depth bins, which could indicate a channel at the base of the surface crevasse field (P4 and/or P5, C2 and/or C3).

At the two downstream sites H1Y15 and H1Y16, the diurnal exchange of meltwater is high throughout the glacier cone. The higher depth-cumulative diurnal meltwater exchange compared with the upstream sites is indicative of downstream meltwater accumulation (via P3 or P4). At both frontal sites, the diurnal meltwater cycle is present at all depths, implying a good hydraulic connection between the surface and the bed (P2). At H1Y15 there is an increase in the diurnal meltwater exchange between ~300- and ~350-m depth. This could be attributed to a ~350-m deep moulin far enough from the ApRES so that it only enters its cone of view at ~300-m depth (P2 and/or C3). At H1Y16 there are three bright spots in the return signal, which again coincide with sharp drops in the vertical profile of the diurnal amplitude and we attribute those to large water-filled englacial channels (C2 or C3).

With only three simultaneous measurements we cannot exclude the possibility that Helheim's bulk water content is constant and that water is simply being rearranged inside the glacier. However, all three 2016 measurements show water gain at the same time of the day, which suggests that the bulk englacial water content is indeed changing diurnally. Much of the deep diurnal signal at the frontal sites was attributed to mechanism P2—moulins, basal crevasses, or network of fractures; however, our observations do not allow us to distinguish between these features. Thus, further measurements, likely requiring a combination of instruments, will be necessary to establish the mechanism responsible for meltwater exchange at all depths.

6. Conclusions

We monitored the interior dynamics of Helheim Glacier and observed strong depth-dependent diurnal variations in the ApRES return signal. We established that the amplitude of the diurnal variations is too large to result from ice dynamics but can be explained by diurnal changes in meltwater inside the glacier. Using the phase of the return signal measured with the high-precision ApRES allowed us to infer and quantify meltwater changes throughout the glacier by comparing the apparent vertical displacement between subsequent internal reflectors. Our results indicate that surface-to-bed connectivity decreases with increasing distance from the glacier terminus and suggest that Helheim's englacial hydrologic network near the front is densely connected, allowing a diurnal meltwater cycle at all depths. We were unable to measure the glacier's background meltwater content and distribution because of the short timespan of our deployment. However, future year-round ApRES observations may reveal the background englacial hydrology structure and its evolution.

Acknowledgments
We are grateful to the support provided from New York University Abu Dhabi through grant G1204, the NASA Jet Propulsion Laboratory Oceans Melting Greenland (OMG) program, and NSF grants ARC-1304137, ANT-0424589, AGS-1338832, and PLR-1443190. DEMs were provided by the Polar Geospatial Center under NSF OPP awards 1043681, 1559691, and 1542736. The GPS and atmospheric data are provided as supporting information. The TRI and ApRES data are too large to be freely stored at a public repository. Therefore, these data are archived at an institutional repository at the New York University's Environmental Fluid Dynamics Laboratory server, and they are freely available upon request to efdl@nyu.edu. We thank Brian Rougeux for deploying on-glacier instruments, and Denise Holland for organizing field logistics. UNAVCO is thanked for maintaining the permanent GPS station HEL2, Annie Zaino for helping with the installation of on-glacier GPS receivers, and Brice Noël for sharing RACMO2.3p2 output. We thank three anonymous reviewers for their insightful feedback.

References

Alley, R. B., Dupont, T. K., Parizek, B. R., & Anandakrishnan, S. (2005). Access of surface meltwater to beds of sub-freezing glaciers: Preliminary insights. *Annals of Glaciology*, *40*, 8–14. https://doi.org/10.3189/172756405781813483

Andersen, M. L., Larsen, T. B., Nettles, M., Elosegui, P., van As, D., Hamilton, G. S., et al. (2010). Spatial and temporal melt variability at Helheim Glacier, East Greenland, and its effect on ice dynamics. *Journal of Geophysical Research*, *115*, F04041. https://doi.org/10.1029/2010JF001760

Bælum, K., & Benn, D. I. (2011). Thermal structure and drainage system of a small valley glacier (Tellbreen, Svalbard), investigated by ground penetrating radar. *Cryosphere*, *5*(1), 139.

Bartholomew, I., Nienow, P., Mair, D., Hubbard, A., King, M. A., & Sole, A. (2010). Seasonal evolution of subglacial drainage and acceleration in a Greenland outlet glacier. *Nature Geoscience*, *3*(6), 408–411. https://doi.org/10.1038/ngeo863

Bartholomew, I., Nienow, P., Sole, A., Mair, D., Cowton, T., & King, M. A. (2012). Short-term variability in Greenland ice sheet motion forced by time-varying meltwater drainage: Implications for the relationship between subglacial drainage system behavior and ice velocity. *Journal of Geophysical Research*, *117*, F03002. https://doi.org/10.1029/2011JF002220

Bell, R. E., Tinto, K., Das, I., Wolovick, M., Chu, W., Creyts, T. T., et al. (2014). Deformation, warming and softening of Greenland's ice by refreezing meltwater. *Nature Geoscience*, *7*(7), 497–502. https://doi.org/10.1038/ngeo2179

Benn, D., Gulley, J., Luckman, A., Adamek, A., & Glowacki, P. S. (2009). Englacial drainage systems formed by hydrologically driven crevasse propagation. *Journal of Glaciology*, *55*(191), 513–523. https://doi.org/10.3189/002214309788816669

Boon, S., & Sharp, M. (2003). The role of hydrologically-driven ice fracture in drainage system evolution on an Arctic glacier. *Geophysical Research Letters*, *30*(18), 1916. https://doi.org/10.1029/2003GL018034

Brennan, P. V., Lok, L. B., Nicholls, K., & Corr, H. (2014). Phase-sensitive FMCW radar system for high-precision Antarctic ice shelf profile monitoring. *Sonar Navigation IET Radar*, *8*(7), 776–786. https://doi.org/10.1049/iet-rsn.2013.0053

Caduff, R., Schlunegger, F., Kos, A., & Wiesmann, A. (2015). A review of terrestrial radar interferometry for measuring surface change in the geosciences. *Earth Surface Processes and Landforms*, *40*(2), 208–228. https://doi.org/10.1002/esp.3656

Catania, G. A., Neumann, T. A., & Price, S. F. (2008). Characterizing englacial drainage in the ablation zone of the Greenland ice sheet. *Journal of Glaciology*, *54*(187), 567–578. https://doi.org/10.3189/002214308786570854

Chen, G. (1998). *GPS kinematic positioning for the airborne laser altimetry at Long Valley California* (PhD dissertation). Massachusetts Institute of Technology.

Colgan, W., Rajaram, H., Abdalati, W., McCutchan, C., Mottram, R., Moussavi, M. S., & Grigsby, S. (2016). Glacier crevasses: Observations, models, and mass balance implications. *Reviews of Geophysics*, *54*, 119–161. https://doi.org/10.1002/2015RG000504

Corr, H. F., Jenkins, A., Nicholls, K. W., & Doake, C. S. M. (2002). Precise measurement of changes in ice-shelf thickness by phase-sensitive radar to determine basal melt rates. *Geophysical Research Letters*, *29*(8), 1232. https://doi.org/10.1029/2001GL014618

Das, S. B., Joughin, I., Behn, M. D., Howat, I. M., King, M. A., Lizarralde, D., & Bhatia, M. P. (2008). Fracture propagation to the base of the Greenland ice sheet during supraglacial lake drainage. *Science*, *320*(5877), 778–781. https://doi.org/10.1126/science.1153360

Davis, J., De Juan, J., Nettles, M., Elosegui, P., & Andersen, M. (2014). Evidence for non-tidal diurnal velocity variations of Helheim Glacier, East Greenland. *Journal of Glaciology*, *60*(224), 1169–1180. https://doi.org/10.3189/2014JoG13J230

de Juan, J., Elósegui, P., Nettles, M., Larsen, T. B., Davis, J. L., Hamilton, G. S., et al. (2010). Sudden increase in tidal response linked to calving and acceleration at a large Greenland outlet glacier. *Geophysical Research Letters*, *37*, L12501. https://doi.org/10.1029/2010GL043289

Everett, A., Murray, T., Selmes, N., Rutt, I. C., Luckman, A., James, T. D., et al. (2016). Annual down-glacier drainage of lakes and water-filled crevasses at Helheim Glacier, southeast Greenland. *Journal of Geophysical Research: Earth Surface*, *121*, 1819–1833. https://doi.org/10.1002/2016JF003831

Fountain, A. G., Jacobel, R. W., Schlichting, R., & Jansson, P. (2005). Fractures as the main pathways of water flow in temperate glaciers. *Nature*, *433*(7026), 618–621. https://doi.org/10.1038/nature03296

Fountain, A. G., & Walder, J. S. (1998). Water flow through temperate glaciers. *Reviews of Geophysics*, *36*(3), 299–328. https://doi.org/10.1029/97RG03579

Gulley, J., & Benn, D. I. (2007). Structural control of englacial drainage systems in himalayan debris-covered glaciers. *Journal of Glaciology*, *53*(182), 399–412. https://doi.org/10.3189/002214307783258378

Harper, J. T., Bradford, J. H., Humphrey, N. F., & Meierbachtol, T. W. (2010). Vertical extension of the subglacial drainage system into basal crevasses. *Nature*, *467*(7315), 579–582. https://doi.org/10.1038/nature09398

James, T. D., Murray, T., Selmes, N., Scharrer, K., & O'Leary, M. (2014). Buoyant flexure and basal crevassing in dynamic mass loss at Helheim Glacier. *Nature Geoscience*, *7*(8), 593–596. https://doi.org/10.1038/ngeo2204

Kulessa, B., Booth, A. D., Hobbs, A., & Hubbard, A. L. (2008). Automated monitoring of subglacial hydrological processes with ground-penetrating radar (GPR) at high temporal resolution: Scope and potential pitfalls. *Geophysical Research Letters*, *35*, L24502. https://doi.org/10.1029/2008GL035855

Lüthi, M., Funk, M., Iken, A., Gogineni, S., & Truffer, M. (2002). Mechanisms of fast flow in Jakobshavn Isbræ, West Greenland: Part III. Measurements of ice deformation, temperature and cross-borehole conductivity in boreholes to the bedrock. *Journal of Glaciology*, *48*(162), 369–385. https://doi.org/10.3189/172756502781831322

Miller, O., Solomon, D. K., Miège, C., Koenig, L., Forster, R., Schmerr, N., et al. (2018). Direct evidence of meltwater flow within a firn aquifer in southeast Greenland. *Geophysical Research Letters*, *45*, 207–215. https://doi.org/10.1002/2017GL075707

Moorman, B. J., & Michel, F. A. (2000). Glacial hydrological system characterization using ground-penetrating radar. *Hydrological Processes*, *14*(15), 2645–2667. https://doi.org/10.1002/1099-1085(20001030)14:15<2645::AID-HYP84>3.0.CO;2-2

Nicholls, K. W., Corr, H. F., Stewart, C. L., Lok, L. B., Brennan, P. V., & Vaughan, D. G. (2015). A ground-based radar for measuring vertical strain rates and time-varying basal melt rates in ice sheets and shelves. *Journal of Glaciology*, *61*(230), 1079–1087. https://doi.org/10.3189/2015JoG15J073

Noël, B., van de Berg, W. J., van Wessem, J. M., van Meijgaard, E., van As, D., Lenaerts, J. T. M., et al. (2018). Modelling the climate and surface mass balance of polar ice sheets using RACMO2 part 1: Greenland (1958–2016). *Cryosphere*, *12*(3), 811–831. https://doi.org/10.5194/tc-12-811-2018

Parizek, B. R., & Alley, R. B. (2004). Implications of increased Greenland surface melt under global-warming scenarios: Ice-sheet simulations. *Quaternary Science Reviews*, *23*(9), 1013–1027. https://doi.org/10.1016/j.quascirev.2003.12.024

Pfeffer, W. T., Humphrey, N. F., Amadei, B., Harper, J., & Wegmann, J. (2000). In situ stress tensor measured in an Alaskan glacier. *Annals of Glaciology*, *31*, 229–235. https://doi.org/10.3189/172756400781820354

Ryser, C., Lüthi, M. P., Andrews, L. C., Hoffman, M. J., Catania, G. A., Hawley, R. L., et al. (2014). Sustained high basal motion of the Greenland ice sheet revealed by borehole deformation. *Journal of Glaciology*, *60*(222), 647–660. https://doi.org/10.3189/2014JoG13J196

Schoof, C. (2010). Ice-sheet acceleration driven by melt supply variability. *Nature*, *468*(7325), 803–806. https://doi.org/10.1038/nature09618

Stuart, G., Murray, T., Gamble, N., Hayes, K., & Hodson, A. (2003). Characterization of englacial channels by ground-penetrating radar: An example from Austre Brøggerbreen, Svalbard. *Journal of Geophysical Research*, *108*(B11), 2525. https://doi.org/10.1029/2003JB002435

Vaughan, D. G., & Arthern, R. (2007). Why is it hard to predict the future of ice sheets? *Science*, *315*(5818), 1503–1504. https://doi.org/10.1126/science.1141111

Voytenko, D., Dixon, T. H., Holland, D. M., Cassotto, R., Howat, I. M., Fahnestock, M. A., et al. (2017). Acquisition of a 3 min, two-dimensional glacier velocity field with terrestrial radar interferometry. *Journal of Glaciology*, *63*(240), 629–636. https://doi.org/10.1017/jog.2017.28

Voytenko, D., Stern, A., Holland, D. M., Dixon, T. H., Christianson, K., & Walker, R. T. (2015). Tidally driven ice speed variation at Helheim Glacier, Greenland, observed with terrestrial radar interferometry. *Journal of Glaciology*, *61*(226), 301–308. https://doi.org/10.3189/2015JoG14J173

Zwally, H. J., Abdalati, W., Herring, T., Larson, K., Saba, J., & Steffen, K. (2002). Surface melt-induced acceleration of Greenland ice-sheet flow. *Science*, *297*(5579), 218–222. https://doi.org/10.1126/science.1072708